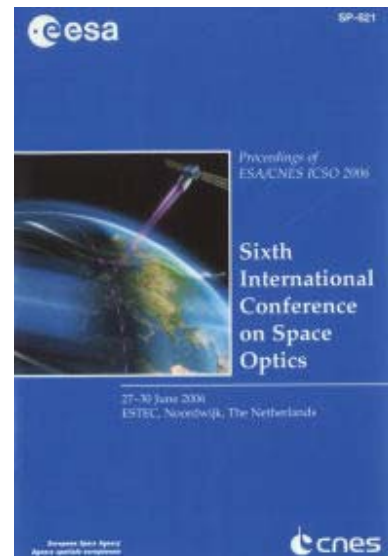


# International Conference on Space Optics—ICSO 2006

Noordwijk, Netherlands

27–30 June 2006

*Edited by Errico Armandillo, Josiane Costeraste, and Nikos Karafolas*



## *Ultra fine measurement of the effect of a vacuum exposure on the central wavelength of narrow-bandpass interference filters manufactured by dual ion beam sputtering*

*Johan Floriot, Frédéric Lemarquis, Morgan Boucanssot, Michel Lequime,*



## ULTRA FINE MEASUREMENT OF THE EFFECT OF A VACUUM EXPOSURE ON THE CENTRAL WAVELENGTH OF NARROW-BANDPASS INTERFERENCE FILTERS MANUFACTURED BY DUAL ION BEAM SPUTTERING

Johan Floriot<sup>(1)</sup>, Frédéric Lemarquis<sup>(1)</sup>, Morgan Boucansot<sup>(1)</sup>, Michel Lequime<sup>(1)</sup>

<sup>(1)</sup>Institut Fresnel, UMR CNRS 6133, Domaine Universitaire de Saint Jérôme 13397 Marseille Cedex 20 (France)

Email: [michel.lequime@fresnel.fr](mailto:michel.lequime@fresnel.fr)

### ABSTRACT

Historically, the optical coating community has greatly improved the environmental stability of interference filters through the incorporation of **energetic processes** into the deposition chamber. This approach brought especially about a stabilization of their spectral features with respect to pressure changes, as occurring during the launching phase in space applications. The objective of our work was to quantify **with a very high resolution** (few picometers) the spectral shift under vacuum exposure of narrow bandpass filters manufactured by Dual Ion Beam Sputtering (DIBS).

We will give first a description of the structure of these filters completed by a presentation of their manufacturing procedure, then a detailed description of our experimental set-up, and at the end a presentation of the results of our measurements on these two specific narrow bandpass filters.

### 1. DESCRIPTION OF THE FILTERS

#### 1.1 Narrow-bandpass filtering

Narrow bandpass filters (i.e. filters with spectral bandwidth less than 1% of the value of the central wavelength) are often used in demanding applications like optical telecommunications, astronomical observation or Raman scattering studies. They can be achieved with the help of two main manufacturing techniques: the first one, hereafter called All Dielectric Fabry-Perot stacks (ADFP), used the deposition of a thin spacer (few microns) between two high reflectance (typically 99.9%) dielectric mirrors including a large number of layers [1]. The second one [2-4] is based on a Solid-Spaced Etalon (SSE), i.e. a quite thin transparent wafer (typical thickness between few tens and few hundred microns) acting as the spacer of a Fabry-Perot cavity and whose both sides are coated with standard performance dielectric mirrors (reflectivity about 95%). This last solution is very attractive in term of number of layers, even if its Free Spectral Range (FSR) can be relatively small (typically 8 nm for a 100-microns SSE around 1550nm), which

obviously limits the range of applications to some specific problems (laser lines stabilization for instance). To increase the width of the rejection band, an efficient way [5-7] is to use auto-filtering cascaded SSE (i.e., for instance, two coherently coupled SSE with different FSR), but the one remains limited to about one hundred nanometers around the design wavelength.

#### 1.2 All-dielectric Fabry-Perot Filter

The design of this first filter can be described by the following formula:

$$\text{Substrate} / \text{M19 2L M19} / \text{Air}$$

where 2L is a half-wave layer of Low index material (silica) and M19 a stack of 19 quarter-wave layers with alternatively High (tantalum pentoxyde,  $n \sim 2.1$ ) and Low (silica,  $n \sim 1.5$ ) index of refraction, i.e.

$$\text{M19} = (\text{HL})^9\text{H}$$

The substrate is a S7006 Schott glass [8], engineered specifically for DWDM (Dense Wavelength Division Multiplexing) applications. The high value of its coefficient of thermal expansion ( $\alpha = 101.10^{-7}/^\circ\text{C}$ ) is used to highly reduce the thermal sensitivity of the central wavelength of the narrow-bandpass filter deposited at its surface [9]. The rear face of the substrate is coated with a standard antireflective stack. The transmission of this ADFP filter, measured with the help of a tunable laser, is shown at the Figure 1.

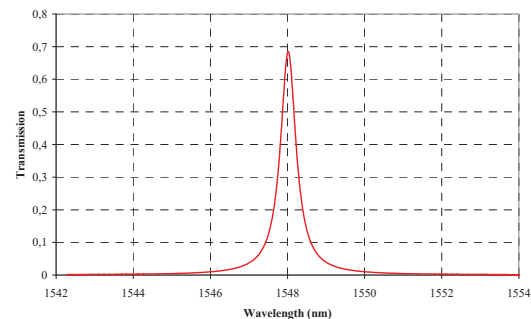


Fig. 1 – Transmission of the ADFP (experimental data)

### 1.3 Solid Spaced Etalon

The cavity of the Fabry-Perot filter is now a silica wafer, with a measured thickness of 49.318 microns [11] and a parallelism better than 2 arc seconds. Each face of this thin substrate is coated with a M9 dielectric mirror, where the high index layers are tantalum pentoxide and the low index layers silica, both deposited through DIBS process. The design of this second filter can be described by the following formula

$$HLHLHLHLH - 184L - HLHLHLHLH$$

where 184L is the thin silica wafer acting in the same time as substrate and cavity. The transmission of this SSE filter, measured with the help of the same tunable laser as used before, is shown at the Figure 2.

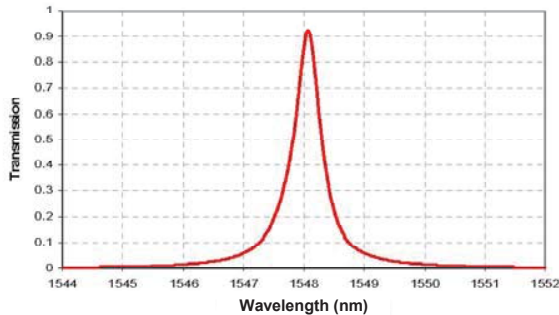


Fig. 2 – Transmission of the SSE (experimental data)

### 1.4 Deposition process

These two filters were manufactured into a vacuum chamber using Dual Ion Beam Sputtering (DIBS) technique (see Figure 3).

A first ion beam (**Ion Beam Sputtering, IBS**) is directed on a plane rotating target tilted at 45° and located at the bottom of the chamber: during the process, we are able to switch this target in order to deposit the two different materials required by the filters design. For the SiO<sub>2</sub> layers, we used a silicon target and a reactive oxygen atmosphere, while for the Ta<sub>2</sub>O<sub>5</sub> layers we used a tantalum target with again the same kind of reactive atmosphere. The sputtered matter condenses at the surface of the substrate which is located at the top part of the same chamber into a rotating holder (rotation axis vertical). This substrate is slightly tilted with respect to a horizontal plane for optimizing the uniformity of the layers thickness. A second ion beam located again at the bottom part of the chamber is directed toward the substrate to compact the matter during the deposition process (**Ion Assisted Deposition, IAD**).

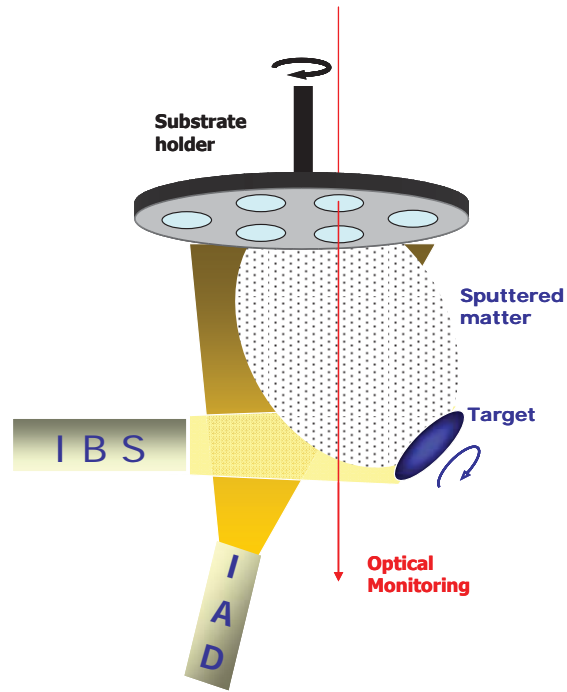


Fig. 3 – The DIBS chamber

The optical thickness of each deposited layer is controlled in real time by an in situ optical monitoring system, which uses as source a tunable laser.

The ion assistance is responsible of the high density of the deposited layers. This lack of porosity for all the layers (and obviously for the cavity in the case of the SSE filter) leads to a potential high stability of the filter performances with respect to air-to-vacuum or vacuum-to-air transitions: it is the reason for which we decided to perform an accurate study of the stability of narrow bandpass filters manufactured with such a high energetic process.

## 2. EXPERIMENTAL SET-UP

### 2.1 Description of the bench

The sample filter is located on a mechanical holder into a small size vacuum chamber, which is equipped with two transparent windows (see Figure 4). A two stages pump is used to ensure a high quality vacuum, the residual pressure being checked in real time with the help of a vacuum gauge.

The sample filter is illuminated through the entrance window by a collimated Gaussian beam whose waist is precisely located on the front face of the filter (diameter of the beam about 0.5mm at 1/e<sup>2</sup>). This Gaussian beam is provided by a singlemode fiber, whose extremity is fixed by gluing near the focal plane

of a grin rod lens. This pigtailed collimator is connected to the output arm of a 3dB-coupler whose input arms are respectively connected to an EXFO FLS-2600 tunable laser source and to an InGaAs photodiode (PD1). The central wavelength of this laser can be tuned between 1520 and 1570nm, by 10pm steps.

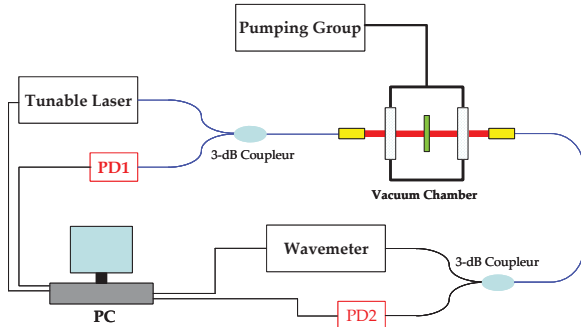


Fig. 4 – The experimental set-up

The light transmitted by the filter is collected, after crossing the exit window, by a second singlemode pigtailed collimator identical to the one previously described. The output extremity of this singlemode fiber is connected to the input arm of a second 3dB-coupler whose output ports are respectively connected to a high resolution wavemeter (resolution better than one picometer) and to a second InGaAs photodiode (PD2). Each photodiode (PD1 and PD2) is followed by a low noise current-voltage amplifier whose gain can be selected between  $10^4$  and  $10^9$  V/A. The output voltage of each amplifier is digitized by a 16-bits analog-to-digital converter and recorded by a Personal Computer. A thermocouple is also used to record the variations of the ambient temperature during the entire test.

## 2.2 Measurement procedure

The measurement procedure is as follows: the spectral transmittance of the filter under test is first measured each 3 hours during few days at ambient pressure. The pumping group is then started to reach a good quality vacuum in the chamber (residual static pressure about  $2.10^{-5}$  mbars). During one week, the transmittance of the filter is again measured each 3 hours in vacuum, then the pressure is slowly increased up to the ambient pressure and the spectral transmittance of the filter is again checked during few days.

To ensure that the changes in the central wavelength of the filter are effectively related to the pressure changes, it is very important to take care to two critical parameters, i.e. the angle of incidence of the beam on the filter and the temperature of this filter. Indeed, in

first approximation, the central wavelength  $\lambda_0$  of a Fabry-Perot filter is defined by the relation (1)

$$2ne \cdot \cos \theta = k\lambda_0 \quad (1)$$

where  $n$  is the refractive index of the cavity,  $e$  its physical thickness,  $k$  an integer and  $\theta$  the angle of incidence inside the filter. The relationship between the angles of incidence inside the filter ( $\theta$ ) and outside the filter ( $\alpha$ ) is defined by a simple Snell-Descartes equation, i.e.

$$\sin \alpha = n \sin \theta \quad (2)$$

It means that the central wavelength of the filter can be affected by a tilt: for instance, in the case of the SSE filter, a rotation of 1 degree is sufficient to induce a change about 100pm on the central wavelength.

On the other hand, any temperature change induces also a modification of the optical thickness  $ne$  of the filter cavity, which has a direct impact on the central wavelength. The thermal sensitivity of the silica is thus given by the relation (3)

$$\frac{1}{ne} \cdot \frac{\partial(ne)}{\partial T} = 7.3 \cdot 10^{-6} / ^\circ\text{C} \quad (3)$$

which leads to a thermal sensitivity about 10 pm/ $^\circ\text{C}$  for the central wavelength of the SSE filter. In the case of the ADFP filter, the use of a S7006 Schott glass as substrate allows to reduce this thermal sensitivity to 4 pm/ $^\circ\text{C}$  (experimental data). It means that the temperature of the filter shall remain stable at  $\pm 1^\circ\text{C}$  during the entire test to limit the thermal noise to less than 10 pm in the worst case (SSE filter).

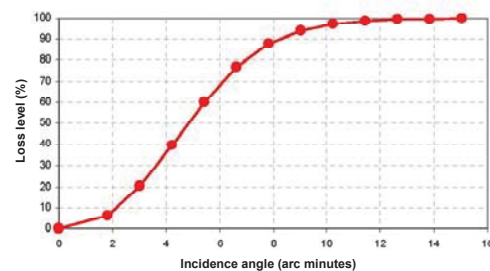


Fig. 5 – Influence of the angle of incidence on the back coupling losses

To cancel the possible influence of the variations of the incidence angle on the central wavelength measurements, we used the following experimental procedure: the filter is first installed on its holder into the vacuum chamber, then the line sight of the input collimator is finely tuned for optimizing the amount of light power measured by the PD1 photodiode. It

guarantees that the illumination beam is perfectly perpendicular to the filter surface. The recording of the variations of the signal delivered by the PD1 photodiode is so used to detect (and quantify) the evolutions of the angle of incidence of the beam on the filter during the test. On the Figure 5, we can see the variations of the back coupling losses with respect to the angle of incidence. These experimental data show that, beyond 10 arc minutes, the coupling losses reach 100%. It means also that, if this loss level is kept under 50% during the test, we can guarantee that the angle of incidence remains smaller than 5 arc minutes, with a related impact on the central wavelength smaller than 1 pm. In fact during all our tests, this loss level remained under 1%.

For extracting the central wavelength of the filter, we used the following data processing approach: the shape of the spectral transmission curve can be always described by an Airy function, i.e.

$$T(\lambda) = \frac{T_0}{1 + A \sin^2 \left[ \pi \frac{\lambda_0}{\lambda} \right]} \quad (4)$$

where  $T$  is the transmission of the filter and  $\lambda$  the wavelength.  $A$ ,  $T_0$  and  $\lambda_0$  are unknown quantities which are determined through the minimization of a merit function  $MF$  (least squares method) defined by

$$MF(T_0, A, \lambda_0) = \frac{1}{N} \sum_{i=1}^N [T_{\text{exp}}(\lambda_i) - T(\lambda_i)]^2 \quad (5)$$

where  $\lambda_i$  is the value of the wavelength measured by the wavemeter for the step number  $i$  of the spectral sweep of the tunable source,  $T_{\text{exp}}(\lambda_i)$  the result of the transmission measurement for this step and  $N$  the number of steps. The Figure 6 shows an example of the result of such a fitting procedure (red crosses: experimental data – blue line: fitted Airy function).

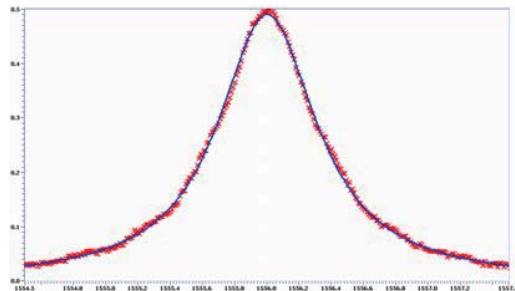


Fig. 6 – Comparison between the experimental transmission data and the fitted Airy function

The accuracy of this method is better than 1 pm on the central wavelength of the filter. To be complete, this

processing method can be also used to determine the spectral bandwidth  $\Delta\lambda$  of the filter (Full Width at Half Maximum), by using the following relation

$$\Delta\lambda = \frac{2\lambda_0}{\pi\sqrt{A}} \quad (6)$$

### 3. EXPERIMENTAL RESULTS

#### 3.1 All-dielectric Fabry-Perot Filter

The Figure 7 shows the results of the central wavelength measurements performed on the ADFP filter during the air-vacuum-air sequence described at the section 2.2.

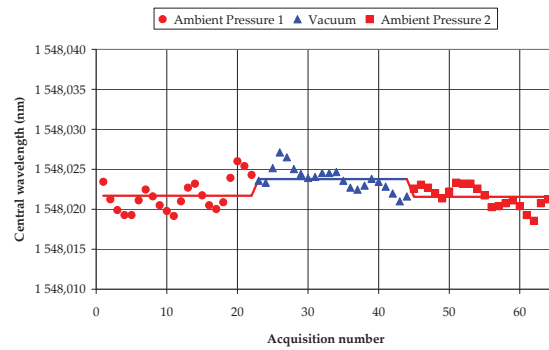


Fig. 7 – ADFP Filter: Results of the central wavelength measurements performed during an air-vacuum-air sequence

The red dots (respectively red squares) are the measurements performed at air before (respectively after) the vacuum exposure (blue triangles). The continuous lines are the mean values of the measurements performed during one part of the whole sequence.

These central wavelength averaged values are as follows:

- Before vacuum exposure: 1548.0217 nm
- During vacuum exposure: 1548.0238 nm
- After vacuum exposure: 1548.0216 nm

We shall stress here the low level of thermal noise on all these central wavelength measurements, as well as the total lack of shift between before and after the vacuum exposure (averaged values identical at 0.1 pm). The shift induced by the vacuum exposure is here equal to +2.1 pm, the positive sign being in accordance with an extremely low residual porosity of the deposited layers.

### 3.2 Solid Spaced Etalon

The results of the measurements performed on the SSE filter during an air-vacuum-air sequence are presented at the Figure 8.

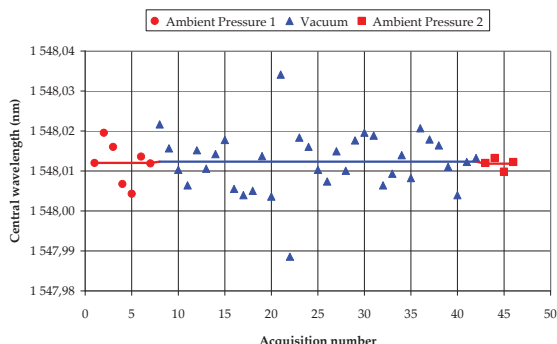


Fig. 8 – SSE Filter: Results of the central wavelength measurements performed during an air-vacuum-air sequence

The fluctuations of the central wavelength measurements around the mean value averaged during one part of the sequence are larger than the ones recorded during the previous experiment, probably because of the higher thermal sensitivity of the filter.

The central wavelength averaged values are as follows:

- Before vacuum exposure: 1548.0120 nm
- During vacuum exposure: 1548.0124 nm
- After vacuum exposure: 1548.0118 nm

The shift induced by the vacuum exposure is here equal to +0.4pm, the reproducibility of the base line being this time about -0.2pm.

### 4. CONCLUSION

The use of a Dual Ion Beam Sputtering technique is able to cancel the effect of a vacuum-to-air or air-to-vacuum transition on the value of the central wavelength of an optical interference narrow-bandpass filter. This deposition technique is also responsible of the high mechanical quality of the layers as well as their strong adhesion on the substrate. By combining the use of this energetic deposition process with the choice of optimized substrates (coefficient of thermal expansion about  $110 \cdot 10^{-7}/^{\circ}\text{C}$ ), it is possible to greatly improve the environmental behaviour of narrow-bandpass filters (with respect to mechanical stresses, temperature changes and vacuum exposure).

### ACKNOWLEDGMENTS

This work was achieved in the framework of a CNES research contract (CNES n° 03/1362/00 – DPI 500).

### 5. REFERENCES

1. H.A. Macleod, *Thin-Film Optical Filters*, Third Edition, Institute of Physics Publishing (2001)
2. J.A. Dobrowolski, *Mica interference filters with transmission bands of very narrow half-widths*, J. Opt. Soc. Am. Vol. 49, 794-806 (1959)
3. R.R. Austin, *The use of solid etalon devices as narrowband interference filters*, Opt. Eng. Vol. 11, 68-69 (1972)
4. A.E. Roche and A.M. Title, *Tilt tunable ultra narrow-band filters for high resolution photometry*, Appl. Opt. Vol. 14, 765-770 (1974)
5. J. Floriot, F. Lemarchand and M. Lequime, *Double coherent solid-spaced filters for very narrow-bandpass filtering applications*, Opt. Comm. Vol. 222, 101-106 (2003)
6. J. Floriot, F. Lemarchand and M. Lequime, *Cascaded solid-spaced filters for DWDM applications*, in Advances in Optical Thin-Films, C. Amra, N. Kaiser and H.A. Macleod, eds., Proc. SPIE Vol. 5250, 384-392 (2003)
7. J. Floriot, F. Lemarchand, and M. Lequime, *Solid-spaced filters: an alternative for narrow-bandpass applications*, Appl. Opt. Vol. 45, 1349-1355 (2006)
8. [http://www.us.schott.com/optics\\_devices/english/products/dwdm.html?highlighted\\_text=7006](http://www.us.schott.com/optics_devices/english/products/dwdm.html?highlighted_text=7006)
9. H. Takashashi, *Temperature stability of thin-film narrow-bandpass filters produced by ion-assisted deposition*, Appl. Opt. Vol. 34, 667 (1995)
10. M. Lequime, *Tunable Thin-Film Filters: Review and Perspectives*, in Advances in Optical Thin-Films, C. Amra, N. Kaiser and H.A. Macleod, eds., Proc. SPIE Vol. 5250, 302-311 (2003)
11. J. Lumeau and M. Lequime, *Localized measurement of the optical thickness of a transparent window: Application to the study of the photosensitivity of organic polymers*, accepted for publication in Applied Optics (2006)